Volume 19, Number 1, 2026. pp. 23-30

Jordan Journal of Physics

ARTICLE

Synthesis, Characterization, and Photocatalytic Activity of Dy_2O_3/Mn Nanostructures

Malek Madani

Laboratory of Physics of Materials and Nanomaterials Applied at Environment (LaPhyMNE), Faculty of Sciences, Gabes University, Tunisia.

DOI: **https://doi.org/10.47011/19.1.3**

Received on: 05/11/2024; *Accepted on: 07/09/2025*

Abstract: The goal of this study is to synthesize and characterize manganese-doped Dy_2O_3 (Dy_2O_3/Mn) nanostructures for catalytic applications. To create materials with optimized morphological and structural properties, a low-cost hydrothermal route was used. Before being characterized, Dy_2O_3/Mn nanostructures were annealed at 500 °C. XRD measurements revealed that sample has a cubic phase structure, with a crystallite size of 37.7 nm. SEM and EDS techniques were used to examine the morphology and chemical composition, and the efficiency of the synthesis route was confirmed. Diffuse reflectance spectroscopy confirmed our samples' absorption in the visible region, and the band gap energy was found to be around 2.87 eV. Methylene blue (MB) dye was used to investigate the photocatalytic activity of Dy_2O_3/Mn nanostructures under visible light. Over six hours, a significant degradation efficiency was observed, with a degradation rate over 80%.

Keywords: Hydrothermal, Dy_2O_3/Mn, Optical properties, Methylene blue, Photocatalysis.

1. Introduction

Addressing environmental pollution is currently receiving significant attention. Organic dyes are major waste pollutants from several sectors, including paper, food, and textiles industries [1, 2]. They are hazardous to humans, wildlife, and vegetation, and have become a serious environmental issue [3]. Methylene blue (MB) was employed as a cationic phenothiazine dye in the textile, printing, and leather industries due to its low energy consumption and simple usage [4]. To remove MB from wastewater, many techniques, including adsorption and catalytic oxidation, have been widely applied [5]. Adsorption, however, may not destroy MB, and some adsorbents have been observed to have low effectiveness and a long processing time [6]. Also, identifying low-cost, high-efficiency, and safe materials, as well as explaining the actual removal process of mixtures for various contaminants in real-life implementations, remains a challenge. Furthermore, methylene blue's strong visible light absorption, self-sensitizing properties, and susceptibility to non-photocatalytic degradation pathways limit its reliability as a model molecule for evaluating photocatalytic activity under visible light. Careful experimental design and complementary analytical techniques are required to distinguish true photocatalytic degradation from dye self-sensitization and other side reactions [7].

Several investigations on the synthesis of mixed oxide catalysts have been conducted, and as a result, a range of manufacturing approaches have been employed. Some of these methods are sol-gel, hydrothermal, co-precipitation, spray pyrolysis, and aqueous wet chemistry [8]. The morphologies and properties of materials, on the other hand, vary significantly depending on the synthesis method and processing conditions. Some of the techniques that could be employed to create Dy_2O_3/Mn nanostructures include microwave-assisted, solid-state, hydrothermal, and polyacrylamide gel [9]. Among these technologies, the hydrothermal method is a straightforward way for producing nanoparticles with controlled and homogenous sizes. This methodology is characterized by its low processing temperature, outstanding

Corresponding Author: Malek Madani **Email**: malek.madani@fsg.u-gabes.tn

homogeneity, simplicity, and cost-effectiveness [10]. In recent years, transition metal oxides, metal sulfides, composite structures, and doped materials have been widely used to catalyze photochemical reactions for environmental remediation [11]. Nonetheless, due to its thermal stability and appropriateness for optical glass, ceramic, and optical applications, dysprosium oxide (Dy_2O_3) has a wide range of uses [12].

The dimensions, shape, and size of materials significantly affect their properties [2]. Consequently, it is imperative to carry out more research on Dy_2O_3, as its unique properties may lead to potential applications [8]. Salavati-Niasari et al.'s publication [9] details $Dy(OH)_3$ nanorods' capacity for photocatalysis. After synthesizing anocrystalline ZnO/Dy_2O_3 using a straightforward chemical process, Joséphine and her associates [12] found that the increased photocatalytic activity was caused by the f-shells in the lanthanide oxide crystal lattice, which trap excited electrons and extend the electron-hole recombination process.

Manganese-doped DyO_3 ($DyMnO_3$) exhibits significant relevance for photocatalytic activity under visible light due to its narrow band gap energy of 2.4 eV, which enables efficient absorption in the visible spectrum. This material achieves rapid and high-efficiency degradation of organic dyes, such as malachite green and methylene blue. The enhanced photocatalytic performance is attributed to effective charge carrier separation and the generation of reactive oxygen species, which actively degrade pollutants. These properties position Mn-doped DyO_3 as a promising visible-light photocatalyst for environmental remediation applications.

Based on the concerns raised above, the hydrothermal method was used to synthesize Dy_2O_3 nanoparticles in this study. Dy_2O_3/Mn materials have oxygen vacancies that can be used to improve photocatalytic activity under visible light and have favorable optical properties [13]. The annealed samples' structural, morphological, and photocatalytic properties were investigated further.

2. Experimental Details

2.1 Sample Preparation

Chemical routes are commonly used to synthesize nanoparticles, mainly because they are the simplest and most cost-effective ways to elaborate such materials. In this work, Dy_2O_3/Mn nanostructure was synthesized using the hydrothermal technique. As illustrated in Fig. 1, $Dy(NO_3)_3.6H_2O$, $Mn(NO_3)_2.4H_2O$, and $C_6H_8O_7$ were mixed in deionized water at an equimolar ratio. Ammonium hydroxide is added dropwise to the solution while stirring for an hour in order to stabilize the citric acid and adjust the pH to approximately 10. This step enables sol formation. The homogenous mixture was then poured into a 60 mL Teflon-lined metal autoclave, which was filled to 80% of capacity. The autoclave was placed in a muffle furnace for 24 hours at 150 °C and left to cool at room temperature. The resulting products were repeatedly rinsed with doubly deionized water and ethanol before being dried at 100 °C overnight. Finally, the obtained powder was calcined at 500 °C for three hours.

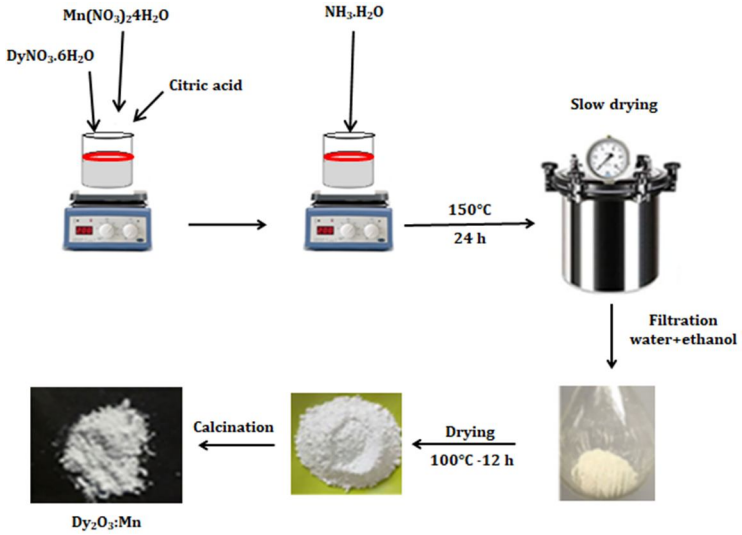

FIG. 1. Schematic illustration of synthesis of Dy2O3/Mn nanopowders.

2.2 Sample Characterization

A variety of characterization techniques were used to analyze the structure, composition, and morphology of the composites. X-ray diffraction measurements were performed using Cu-K radiation (XRD, Bruker D-8 Advance Diffractometer). The FEI-NOVA-NANOSEM/450 was used for scanning electron microscopy (SEM) and energy dispersive spectroscopy (EDS) to characterize the surface morphology and elemental composition of the sample. The optical properties of composite materials were investigated using a UV-visible spectrophotometer (HALO-DB-20 UV-Vis spectrophotometer).

2.3 Photocatalytic Activity

The photocatalytic activity of Dy_2O_3/Mn nanostructures was determined by observing the degradation of methylene blue (MB) in aqueous solution under visible light irradiation. At room temperature, photodegradation of MB organic dye was carried out in a glass vial (30 mL) placed on a magnetic hotplate stirrer with a stirring rate of 280 rpm in the presence of the fabricated Dy_2O_3/Mn nanostructures. The reaction was carried out in 100 mL of 10 ppm MB solution with 0.1 g of Dy_2O_3/Mn nanostructures and 15% H_2O_2. Since MB is stable in the dark but photosensitive to visible light, and Dy_2O_3/Mn suspension has a strong ability to respond to light and CO_2 in air, both were kept in the dark before the reaction. After one hour, the suspensions were exposed to light and stirred regularly. MB degradation was detected in a UV-VIS spectrophotometer by removing aliquots of the reaction mixture at regular intervals. The degradation percentage of the dye solution was calculated using the model [14]:

$$Degradation\ \eta(\%) = \frac{C_0 - C}{C_0} \times 100 \qquad (1)$$

where C_0 and C are the initial and the variable reaction concentrations (ppm).

3. Results and Discussion

3.1 Crystal Structure

Figure 2 depicts the XRD patterns of Dy_2O_3/Mn nanostructure calcined at 500 °C. The entire diffraction pattern is quite similar to the characteristic (JCPDS 86-1327) standard for Dy_2O_3 characteristics [15]. The pattern revealed the presence of nine distinct peaks, which correspond to the planes (211), (222), (400), (411), (332), (134), (125), (440), and (611), respectively, at 2θ = 20.37°, 29.24°, 33.62°, 35.66°, 39.67°, 43.31°, 48.33°, 50.04°, and 53.01° of the cubic phase structure. The sharpness and intensity of the diffraction peaks indicate the formation of the Dy_2O_3/Mn structure at 500 °C. The diffraction peak observed at 2θ = 26.78° and marked with the ‘’*’’ symbol in the diffraction pattern is does not belong to the cubic structures of both Dy_2O_3 and Mn_2O_3 phases. This diffraction peak is assigned to the formation of the Dy-O-Mn structure. Structural parameters were refined according to the Rietveld method using the FullProf software as illustrated in Fig. 3. The reliability factors were R_p: 16.9%, R_{wp}: 22.4%, R_{exp}: 16.90% and χ^2: 1.75.

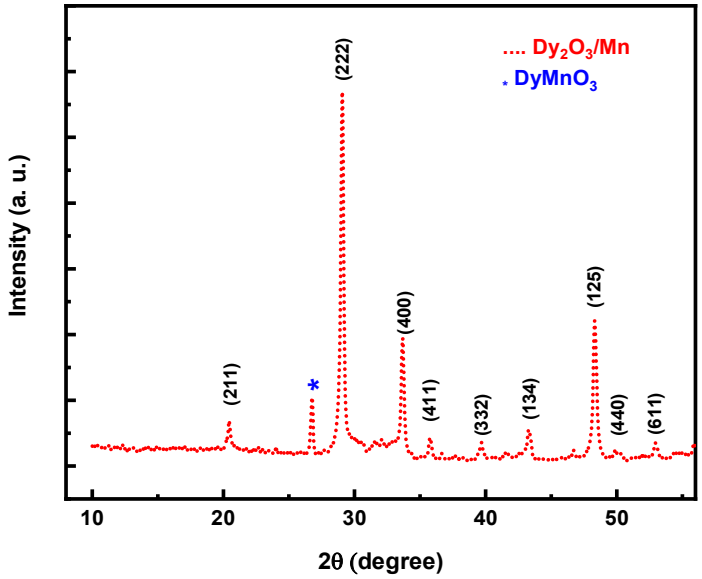

FIG. 2. X-ray diffraction pattern of Dy_2O_3/Mn nanostructure.

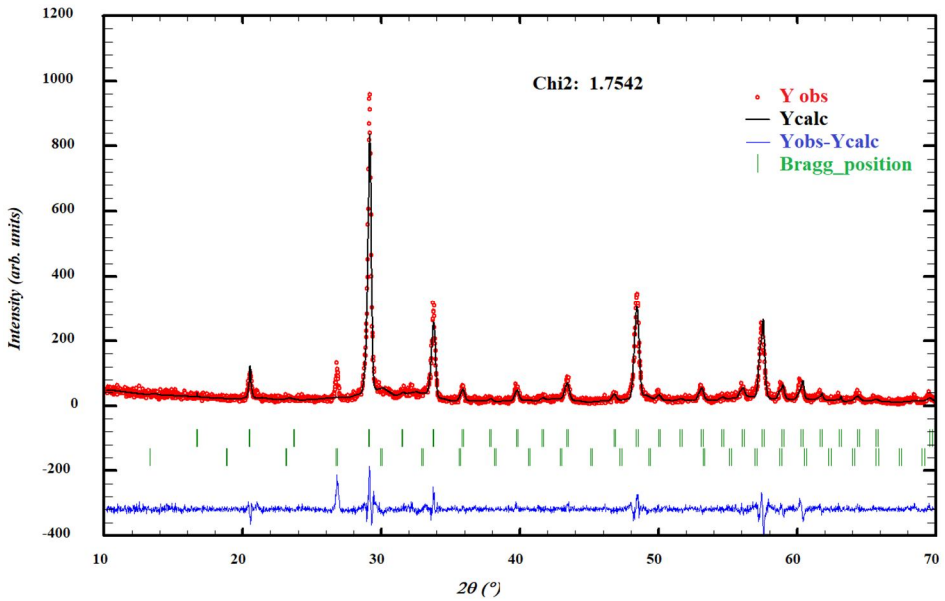

FIG. 3. The Rietveld refinement of the Dy_2O_3/Mn X-ray diffraction pattern

The refinement proved the coexistence of two phases Dy_2O_3 and Mn_2O_3 in the sample. All structural parameters are summarized in Table 1. These results are in concordance with those obtained for samples elaborated by co-precipitation or green combustion routes confirming the efficiency of the hydrothermal technique used in this work [16].

An increase in temperature enhances crystallinity, which would cause the diffraction peak to gradually weaken. Rajendran et al. [17] prepared (Nd, Ce)-doped Dy_2O_3 nanoparticles by hydrothermal method. They have reported that all the samples show high quality with excellent crystallinity. The crystallite size (D) was estimated from the Scherrer's equation [18]:

$$D = \frac{0.9\lambda}{B\cos\theta} \quad (2)$$

where λ is the X-ray wavelength (1.5418 Å), θ is the Bragg diffraction peak and B is the full width at half maximum (FWHM in radians). The crystallite size estimation deduced from the most intense peak (222) was found to be around 37.7 nm.

TABLE 1. Structural parameters of both Dy_2O_3 and Mn_2O_3 phases according to the Rietveld refinement

Dy_2O_3
Phase (space group): Cubic (Ia3)
Cell parameters: a=10.63 Å
Volume: 1201.32 $Å^3$
Density: 7.963 $g.cm^{-3}$
Atom positions:
Name x y z B occ. Mult.
Mn1 0.08879(0) 0.08879(0) 0.08879(0) 0.000(0) 0.300(0) 8
Mn2 0.62391(0) 0.00000(0) 0.25000(0) 0.000(0) 0.300(0) 12
Mn3 0.81854(0) 0.00000(0) 0.25000(0) 0.000(0) 0.500(0) 12
O1 3.15632(0) 2.33679(0) 2.56938(0) 0.000(0) 1.000(0) 24
O2 0.24645(0) 0.97997(0) -0.75461(0) 0.000(0) 1.000(0) 24
Mn_2O_3
Phase (space group): Cubic (I-21-3)
Cell parameters: a=9.42 Å
Volume: 836.526 $Å^3$
Density: 4.893 $g.cm^{-3}$
Atom positions:
Name x y z B occ. Mult.
Dy1 0.25000(0) 0.25000(0) 0.25000(0) 0.000(0) 0.239(4) 8
O1 0.38355(269) 0.10104(257) 0.65620(254) 0.000(0) 1.612(60) 48
Dy2 -0.03162(34) 0.00000(0) 0.25000(0) 0.000(0) 0.673(5) 24

3.2 Morphology and Chemical Composition

Scanning electron microscopy (SEM) was used to analyze the morphological properties of the samples in order to examine the effects of shape, morphology, and size. As demonstrated in Fig. 4(a), the SEM images of Dy2O3/Mn calcined at 500 °C display an agglomerated form with no discernible size distribution. Fig. 4(b) displays the elemental mapping and the EDS spectra of the sample. As with XRD measurements, no other elements are detected besides oxygen, dysprosium, and manganese, which confirm the high purity of the sample and the reliability of the elaboration process.

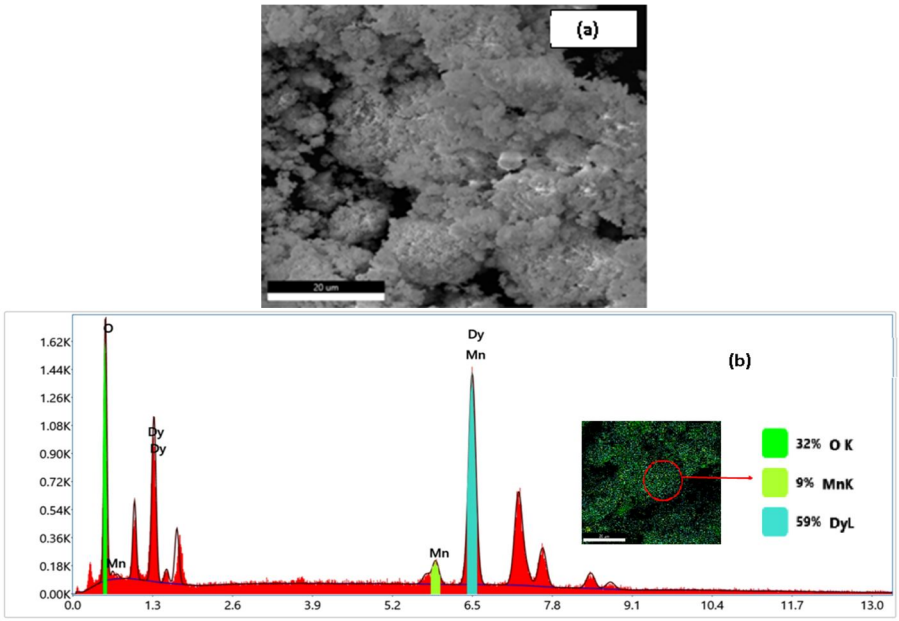

FIG. 4. SEM images (a), elemental mapping and EDS spectra (b) of the Dy_2O_3/Mn structure.

3.3 Optical Properties

The diffuse reflectance spectroscopy (DRS) of Dy_2O_3/Mn nanostructures calcined at 500 °C in the UV-visible range is shown in Fig. 5. The reflectance edge lies in the UV range, which corresponded to the sample's optical band gap. The optical band gap (Eg) was calculated using the Tauc relation [19] and plotting $(\alpha h\nu)^2$ versus $(h\nu)$ (Fig. 6). The band gap energy Eg is found to be 2.89 eV. This Eg value of the calcined sample is comparable to previous works. According to Rajendran et al. [17], the increase in band gap is due to the quantum confinement effect caused by smaller crystallites. It has the potential to be used in photoconductive and photothermal applications. The literature shows that a rise in energy band gap can be attributed to an increase in carrier concentration, grain size, and oxygen vacancies, [20]. The expanding size of the nanoparticles is primarily responsible for the increase in optical band gap in this case. The quantum confinement effect, in fact, causes the gap energy for quantum dots to be inversely proportional to crystallite size [21].

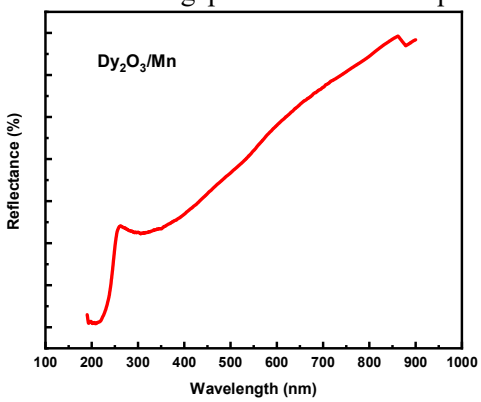

FIG. 5. Diffuse reflectance spectrum of the Dy_2O_3/Mn nanostructure.

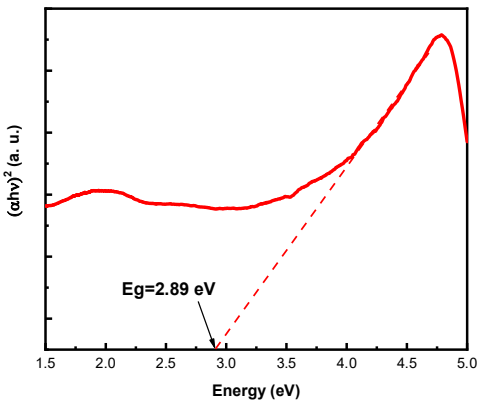

FIG. 6. Tauc plot of the Dy_2O_3/Mn nanostructure and determination of Eg value.

3.4 Photocatalytic Activity

Methylene blue (MB) is generally considered a representative organic dye in textile effluents, which can be easily monitored by optical absorption spectroscopy [22]. In this work, MB was chosen as a model contaminant in photocatalytic decomposition to evaluate the photocatalytic activities of nanocomposites under visible light illumination. As can be observed in Fig. 7, a high MB degradation efficiency (over 80% after 6 hours) was obtained with Dy_2O_3/Mn nanocomposite annealed at 500 °C.

The absorption spectra illustrated by Fig. 8 demonstrate that the adsorption of MB at 664 nm nearly disappeared and the blue color of the solution completely disappeared after the MB solution was irradiated for six hours. The possible reason for the improved photodegradation efficiency of MB with the sample calcined at 500 °C could be due to the significant absorption of visible light, higher charge carrier separation, and an ensuing diffusion of carriers on the surface of photocatalysts. The arrangement of the composite structures may decrease the recombination of hole and electron pairs on the catalyst surface and, therefore, affect the degradation process as illustrated in the proposed mechanism in Fig. 10.

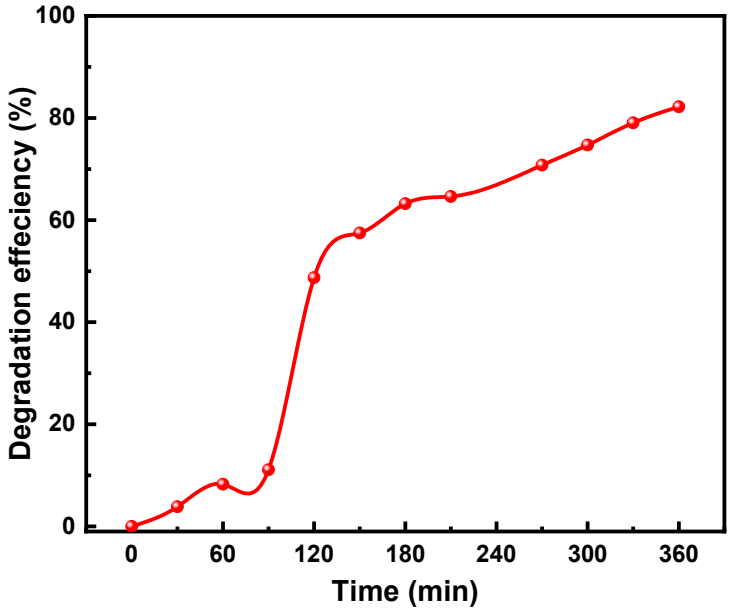

FIG. 7. Degradation efficiency of MB dyes under visible light using Dy_2O_3/Mn nanostructure

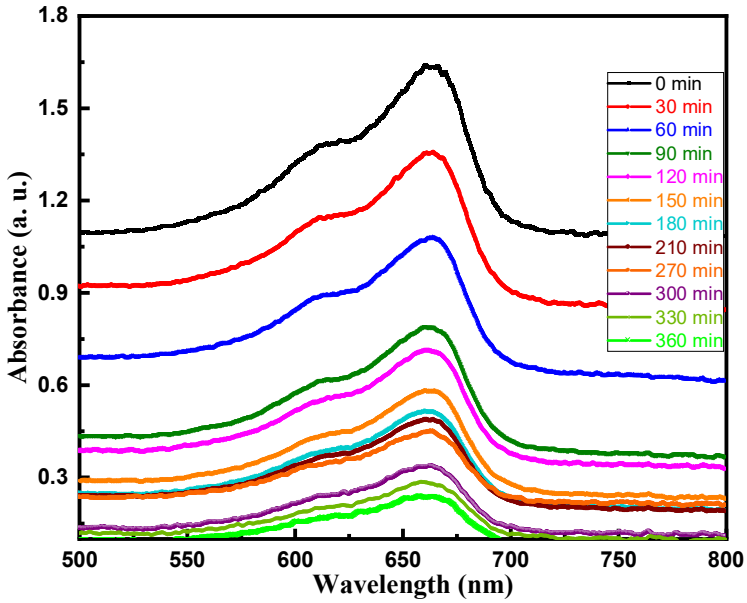

FIG. 8. Time dependence of the MB absorption spectrum dyes in presence of Dy_2O_3/Mn nanostructure.

The photodegradation kinetics of MB was fitted to the pseudo-first-order model [23], as shown in the following equation.

$$\ln \frac{C_0}{C} = k_{app} t \quad (3)$$

where C_0 and C are the initial and final concentrations of MB at standard time periods and k_{app} is the apparent pseudo first-order rate constant (min^{-1}) and t is the light irradiation time (min). The linear relationship between $\ln(C_0/C)$ versus irradiation time are shown in Fig. 9. From this dependence, we found that a first-order reaction is confirmed. The apparent rate constant (k_{app}) is found to be equal to 467 x 10^{-5} min^{-1}.

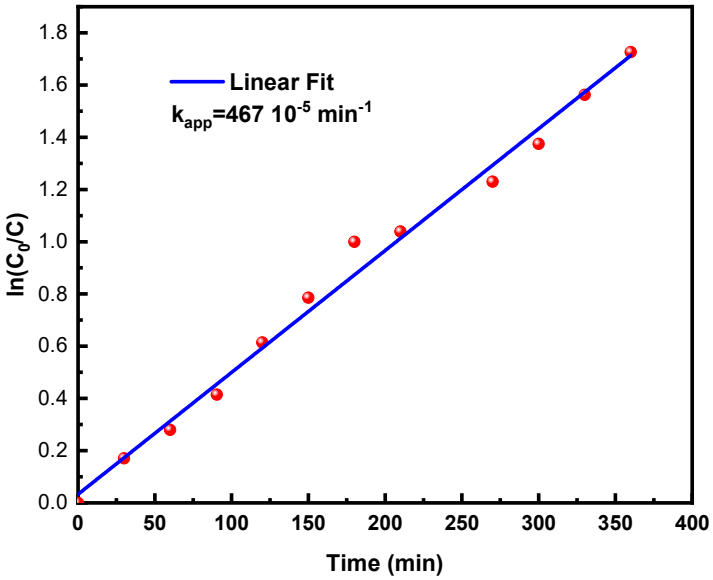

FIG. 9. Kinetics of MB degradation efficiency of MB dyes under visible light with Dy_2O_3/Mn nanostructure.

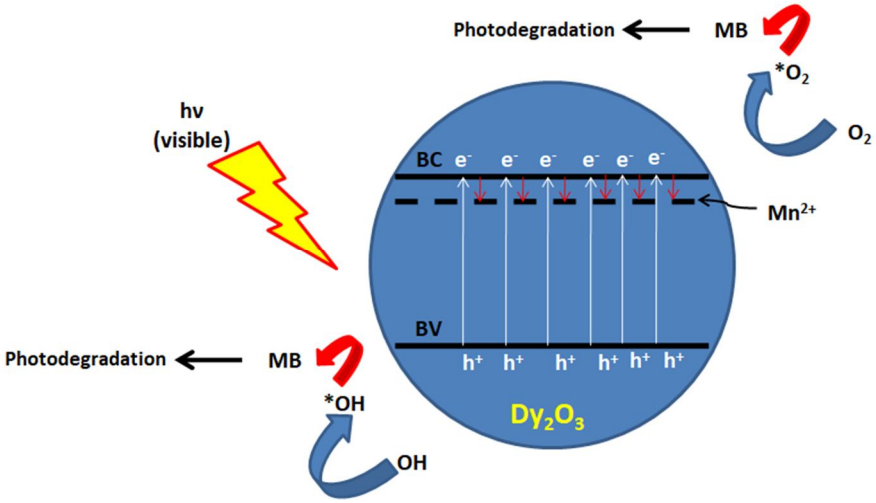

FIG. 10. The proposed mechanism for the photocatalytic decolourization of MB dye over of Dy_2O_3/Mn nanostructures under visible irradiation.

4. Conclusion

In conclusion, the hydrothermal technique and raw materials such as dysprosium oxide, nitric acid, citric acid, and manganese acetate, were suitable for synthesizing of Dy_2O_3/Mn nanostructure. XRD showed the formation of the Dy_2O_3 phase, and SEM images showed the porous surface morphology as well as the presence of nanoparticles. The optical energy band gap of the sample was measured using UV-Vis absorption spectroscopy, and it was discovered that the band gap (2.87 eV) is intimately linked with the particle size (37.7 nm). For photodegradation of MB under visible light radiation, Dy_2O_3/Mn nanostructures calcined at 500 °C exhibited promising performances. The photodegradation efficiency was over 80% after six hours of illumination. The photodegradation kinetics of MB was fitted to the pseudo-first-order model, and the apparent rate constant was 467 x 10^{-5} min^{-1}.

References

[1] Panahi, A., Monsef, R., Imran, M.K., Abdul Mahdi, A., Ruhaima, A.A., and Salavati-Niasari, M., International Journal of Hydrogen Energy, 48 (2023) 3916.

[2] Madani, M., Mansour, H., Omri, K., Gouadria, S., and El Mir, L., European Physical Journal - Plus, 138 (8) (2023) 720.

[3] Gholami, T., Salavati-Niasari, M., and Varshoy, S., International Journal of Hydrogen Energy, 42 (2017) 5235.

[4] Salavati-Niasari, M., Farzaneh F., and Ghandi, M., Journal of Molecular Catalysis A: Chemical, 186 (2002) 101.

[5] Hooda, A., Khatkar, S.P., Khatkar, A., Malik, R.K., Dalal, J., Devi, S., and Taxak, V.B., Materials Chemistry and Physics, 232 (2019) 39.

[6] Alonizan, N., Chouiref, L., Omri, K., Gondal, M.A., Madkhali, N., Ghrib T., and Alhassan, A.I., Journal of Inorganic and Organometallic Polymers and Materials, 30 (2020) 4372.

[7] Mohamed, R.M., Mkhalid, I.A., Baeissa, E.S., and Al-Rayyani, M.A., Journal of Nanotechnology, 2012 (2012) 329082.

[8] Madani, M., Omri, K., Echabaane, M., Gouadria, S., and Alharbi, F., Applied Physics A: Materials Science and Processing, 127 (6) (2021) 435.

[9] Salavati-Niasari, M., Javidi, J., and Davar, F., Ultrasonics Sonochemistry, 17 (2010) 870.

[10] Her, J.L., Pan, T.M., and Lu, C.H., Thin Solid Films, 520 (2012) 5706.

[11] Madani, M., Mansour, H., Alonizan, N., and Omri, K., Chemistry Africa, 7 (2024) 1585.

[12] Josephine, G.A.S. and Sivasamy, A., Applied Catalysis B: Environment and Energy, 288 (2014) 150.

[13] Alonizan, N., Madani, M., Omri, K., Abumousa, R.A., Alyami, A.A., Alqahtani, M.E., Almarri, H.M., and Algrafy, E.M., European Physical Journal - Plus, 2023 (2023) 138.

[14] Chauhana, R., Kumar, A., and Chaudharya, R.P., Applied Surface Science, 270 (2013) 655.

[15] Xu, A.W., Fang, Y.P., You, L.P., and Liu, H.Q., Journal of the American Chemical Society, 125 (2003) 1494.

[16] Chandrasekhar, M., Nagabhushana, H., Sudheerkuma, K.H., Dhananjaya, N., Kavyashree, D., Shivakumara, C., and Nagabhushana, B.M., Materials Research Bulletin, 55 (2014) 237.

[17] Rajendran, V. and Mekala, R., Journal of Alloys and Compounds, 741 (2018) 1055.

[18] Madani, M., Omri, K., Fattah, N., Ghorbal, A., and Portier, X., Journal of Materials Science: Materials in Electronics, 28 (17) (2017) 12977.

[19] Omri, K., Najeh, I., Dhahri, R., El Ghoul, J., and El Mir, L., Microelectronic Engineering, 128 (2014) 53.

[20] Omri, K. and Gouadria, S., Journal of Materials Science: Materials in Electronics, 32 (2021) 17021.

[21] Omri, K., Gouadria, S., Madani, M., Alonizan, N., and Alharbi, F., Journal of Materials Science: Materials in Electronics, 34 (5) (2023) 444.

[22] Oladoye, P.O., Ajiboye, T.O., Omotola, E.O., and Oyewola, O.J., Results in Engineering, 16 (2022) 100678.

[23] Aisien, F.A., Amenaghawon, N.A., and Ekpenisi, E.F., Journal of Engineering and Applied Science, 9 (2013) 11.